New Raman Water Vapor and Temperature Lidar at JPL Table Mountain Facility: Optimization, Validations and Sonde Intercomparison

R.A.Aspey, I.S.McDermid, T.Leblanc, D.Walsh & J.Howe

Jet Propulsion Laboratory, California Institute of Technology,
Table Mountain Facility, P.O.Box 367, 24490 Table Mountain Road,
Wrightwood CA 92397 U.S.A.

ABSTRACT

Jet Propulsion Laboratory currently operates lidar systems at Table Mountain Facility (TMF), California (34.4°N, 117.7°W at 2300m) and Mauna Loa Observatory (MLO), Hawaii (19.5°N, 155.6°W at 3400m) under the Network for the Detection of Atmospheric Composition Change (NDACC, formerly NDSC). To complement existing NDACC lidars at TMF, which acts as a primary site for inter-comparisons, a new water vapor and temperature lidar has begun routine operation with typically 3-4 nightly profiles per week. As water vapor is a key greenhouse gas, and is highly variable on annual and seasonal cycles, accurate long term measurements are necessary for predictions of climate change and to increase our understanding of the atmospheric processes it contributes to. The new TMF lidar has demonstrated high spatial and temporal resolution, with a high degree of optimization being achieved over the past year, although the authors believe further improvement may yet be possible. The lidar has been designed for accuracies of 5% up to 12km in the free troposphere with the capability to measure to the tropopause and lower stratosphere with accuracies of 1 ppm. It is anticipated that the data sets produced will be used for Aura validation and for incorporation into NDACC archives. Validation results for the optimized system are presented with intercomparisons using Vaisala RS92-K radiosondes.

Keywords: Raman, Lidar, Water Vapor, Troposphere

1. INTRODUCTION

Water vapor in the troposphere and lower stratosphere plays a major role in the radiative budget of the earth due to the strongly absorbing nature of the water molecule in the 100-600cm^{-1} infrared region; it absorbs more radiation than CO_2 and contributes to between 27 and 35% of greenhouse forcing.[1–4] The spatial and temporal distribution of tropospheric water vapor is highly variable and inadequacies in middle and upper tropospheric water vapor climatologies are widely reported due to poor radiosonde performance in cold dry conditions and limitations of lidar water vapor measurements.[5,6] Although present in small amounts water vapor plays a major role in atmospheric photo-chemistry[1,6] and thus accurate measurements of lower stratospheric water vapor are important for validation of satellite instrumentation (e.g. EOS-Aura) as well as chemical transport and radiative transfer models. Water vapor in the stratosphere has its origins in photochemical oxidation of methane, upwelling across the tropical tropopause and Brewer-Dobson circulation, while tropospheric water vapor is controlled by local climatic and seasonal variations.[1] Although the quantities of UTLS water vapor are small, they are known to have a disproportionately large effect per molecule ($\times$100) compared to the free troposphere.[1] Another important variable in the hydrological cycle is temperature since the capacity of a parcel of air to hold water vapor (and hence mixing ratio) is related to temperature via saturation mixing ratio w_s. Various Raman water vapor lidars have been described in the literature that have shown limited sensitivity to very low mixing ratios found in the upper troposphere-lower stratosphere (UTLS) region.[1,8–11] To address these issues a new Raman

Further author information: (Send correspondence to R.A.Aspey)
R.A.Aspey: E-mail: aspey@tmf.jpl.nasa.gov, Telephone: +1 760 249 6176
T.Leblanc: E-mail: leblanc@tmf.jpl.nasa.gov Telephone: +1 760 249 1070
SPIE Lidar Remote Sensing Conference, Stockholm 2006.

lidar has been developed at Table Mountain Facility. The TMF Raman lidar measures temperature below 30km using vibrational Raman N_2 (387nm) backscatter and up to 85km using Rayleigh integration (355nm) with the assumptions that the atmosphere is an ideal gas in hydrostatic equlibrium. Water vapor mixing ratio is measured at TMF to a maximum geometric altitude of 18km (site level is 2.3km) with typically 3-4 measurements per week with coincident profiles from Vaisala RS92-K radiosondes. The focus of this paper is the validation of preliminary water vapor lidar results from a six month period using radiosondes; measurements of temperature will not be discussed further.

2. RAMAN LIDAR THEORY

Raman scattering is characterized by a shift in wavelength relative to the exciting (laser) wavelength that is proportional to the distinct rotational-vibrational energy levels of a given molecule. Pure rotational Raman (PRR) contains two branches the S (Stokes) and O (anti-Stokes) that are approximately equal in amplitude and symetrical about the exciting (Rayleigh/Cabannes) line. PRR lidar offers larger signal returns compared to vibrational Raman although yielding a smaller wavelength shift and requiring far higher (10^{10}) rejection of out-of-band (up to 3.5%) interference than vibrational Raman due to the proximity of the Rayleigh/Cabannes line.[9,12] For atmospheric species the shift is to longer wavelengths (Stokes Raman) with the advantage compared to DIAL lidar that emission wavelength does not have to be tuned.[9] As atmospheric Nitrogen is present in constant proportion to 85km (78.084%) normalising the H_2O (407nm) Raman return with the N_2 (387nm) Raman profile allows mixing ratio to be calculated (assuming single scattering). The vibrational spectrum of N_2 and H_2O correspond to transition $v = 0 \rightarrow 1$ and a shift ν_r of 2330.7cm^{-1} and 3652cm^{-1} respectively from the exciting wavelength λ_L where the Raman wavelength is given by $\lambda_r = (1/\lambda_L - \nu_r)^{-1}$.[20] The technique compensates for variations in laser energy, field of view overlap[13,14] and is inherently immune to the presence of aerosols which may be present to altitudes of 30km. Accurate calibration is, however, required although once calibration has been completed good long term stability is possible.[15,16] For an ideal Raman lidar system, where the channel efficiencies ξ_w and ξ_n are equal and signal returns directly represent molecular quantities, water vapor mixing ratio in g/Kg may be calculated from $w = 0.485 \times N_w(z)/N_n(z)$ where $N_w(z)/N_n(z)$ is the ratio of molecular densities.[7] Due to the dominance of sky noise in Raman measurements it has been shown that maximum pulse energy is more important than average power as the background noise is relatively constant and cannot be reduced significantly by averaging. Corrections are also required for differential transmission $\Delta\tau(\lambda_n, \lambda_w, z)$ of molecular N_2 and H_2O due to the λ^{-4} dependence of transmission $T(z)$. Additionally, due to the very low signal levels, noise of tens of mV may become significant requiring stringent screening and ground loop protection, while compensation is required for pulse pileup and signal induced noise (SIN) in Rayleigh channels.[17] The correction for pulse pile-up is given by $N_z = N_m/(1 - (N_m\rho/T_s))$ where N_r is the real count rate, N_m is the measured count rate, ρ is the resolving (dead time) and T_s is the total counting time (bin width times number of shots).[18–20] The general equation for a monostatic Rayleigh/Mie lidar return at a wavelength λ with a backscatter coefficient β_λ is given by[21,22]

$$P(z) = P_o\left(\frac{c\tau}{2}\right) A z^{-2} \beta_\lambda(z) \exp\left\{ -2 \int \alpha(z)\, dz \right\} \tag{1}$$

where P_o is the transmitted power, $c\tau$ is the pulse length, A is the detector area, $\beta(z)$ is the volume backscatter coefficient and $\alpha(z)$ is the volume extinction coefficient due to molecular and aerosol contributions; the characteristic z^{-2} signal variation with height is accounted for by a decrease in solid angle of the receiver. For a biaxial lidar having overlap $O(z)$ where the inelastic return wavelength λ_r differs from the laser wavelength λ_L

$$P(z, \lambda_L, \lambda_R) = P_o(\lambda_L)\frac{k^*}{z^2} O(z)\beta(z, \lambda_L, \lambda_R) \exp\left\{ -\int_0^z [\alpha_L(\lambda_L, z) + \alpha_R(\lambda_R, z)]\, dz \right\} \tag{2}$$

where k^* is the lidar calibration constant and α_L and α_R refer to extinction coefficients (m^{-1}) due to laser and Raman scattering returns respectively. The backscatter coefficient is given by $\beta_{wv}(z) = N_{wv}(z) \times \sigma_{wv}$ ($m^2.sr^{-1}$), where $N_{wv}(z)$ is the molecular number density and σ_{wv} is the Raman water vapor cross sectionwhere the

elastic backscatter term β_λ is replaced with the inelastic Raman cross section $d\sigma/d\Omega$ ($m^2.molecule^{-2}.sr^{-1}$) and extinction at the Raman shifted wavelength is added[6] together with B is the sky background contribution.[21,22]

$$P(r) = P_o(\lambda_L)\frac{c\tau}{2}\frac{k^*}{z^2}O(z)N(z)\frac{d\sigma}{d\Omega}\exp\left\{-\int_0^z[\alpha_L(\lambda_L,z)+\alpha_R(\lambda_R,z)]\,dz\right\}+B \tag{3}$$

The Raman backscatter coefficient is related to the scattering cross section $d\sigma/d\Omega$ of the molecule by the number density where[22] $\beta(z,\lambda_L,\lambda_R) = N(z)\frac{d\sigma(\lambda_L,\lambda_R)}{d\Omega}$.

3. TMF RAMAN LIDAR AND OPTIMIZATIONS

The configuration of the TMF Raman lidar system is illustrated in Figure 1. The left figure shows the receiver and Nd:YAG frequency multiplied transmitter (355nm) configuration and the right figure shows the filter polychromator.* The optical arrangement of the filter polychromator is shown in Figure 2. where the small telescopes are used for correction of field of view overlap function due to the narrow field of view (NFOV) of the 0.92m Newtonian telescope. Uncorrected signals for the lidar are shown in Figure 3. for both narrow and wide field channels; the gated signal from the 355H channel is omitted for clarity. It can be seen that the WFOV signals reach steady state rapidly below 10km but with a large offset due to a larger sky background contribution. The 1σ statistical uncertainty due to Poisson statistical error in photon counting is also indicated which ultimately determines measurement uncertainty.

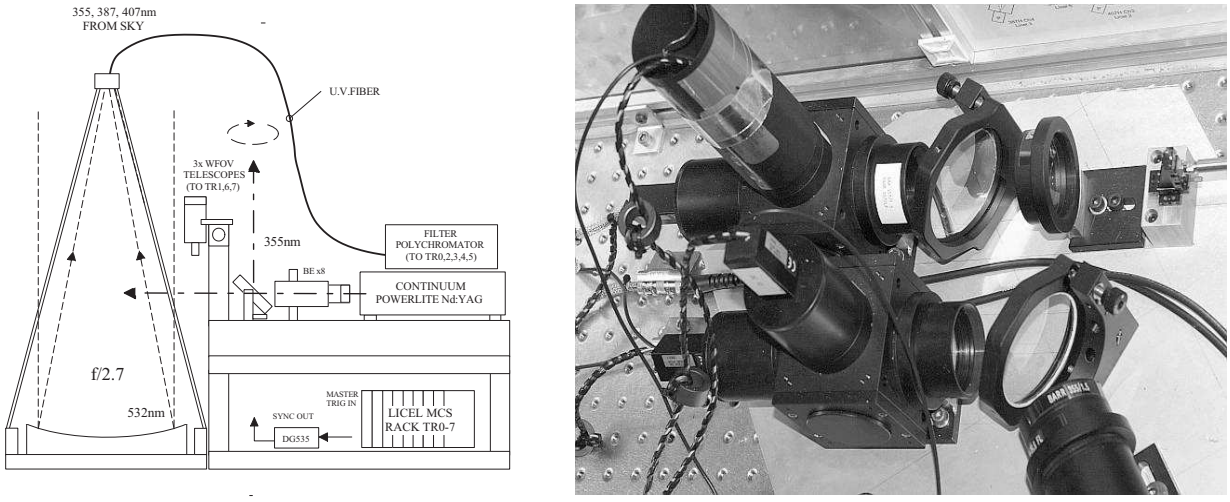

Figure 1. TMF Raman lidar system (left) showing biaxial configuration with three WFOV 7.5cm galilean telescopes and single NFOV 92cm Newtonian telescope and (right) filter polychromator showing optical fiber, aperture stop, dichroic beam splitters, filter housings and PMT's. Note the torroids on PMT power leads to suppress parasitics oscillations.

The data acquisition system employs eight Licel TR20-160 photon counting multi-channel scaler (MCS) modules which simultaneously acquire profiles due to them sharing a common trigger, with a maximum of 16380 bins (124km). Each module has a bandwidth of 250MHz with a minimum dwell time of 50nm (7.5m), although for measurement of water vapor the maximum altitude was 18km with a resolution of 75m (1638 bins). Data transfer uses a National Instruments PC-DIO-32HS data acquisition (I/O) card that interfaces the Licel rack to the acquisition PC. Each transient recorder incorporates a separate discriminator and preamplifier with signals from seven Hamamatsu H5783P PMT's and a single Hamamatsu R7400 PMT are coupled to the Licel rack via coaxial cable. Gating the R7400 PMT during high intensity near field returns on channel 355H (Figure

*While it is preferable to operate at shorter wavelengths since $ds/d\Omega$ varies as λ^{-4}, wavelengths below 248nm are avoided as these coincide with the Hartley ozone absorption band.

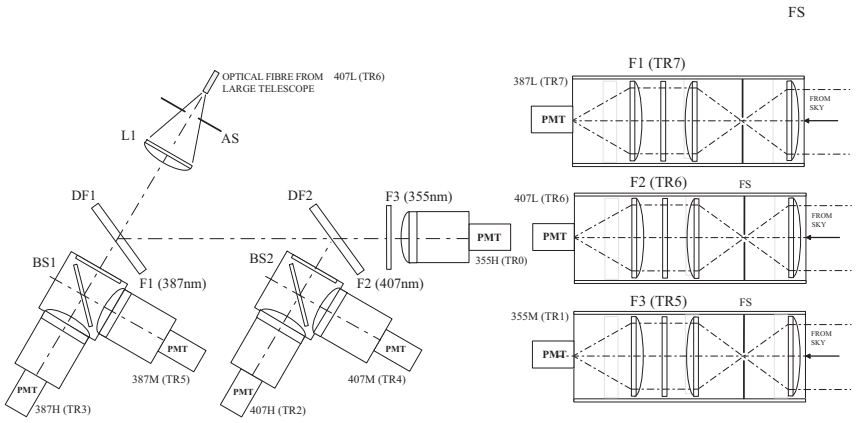

Figure 2. Polychromator optical arrangement for narrow field of view (NFOV) 0.92m telescope polychromator and three 7.5cm wide field of view (WFOV) telescopes for 387L, 407L and 355M channels. PMT's to Licel transient recorder modules TR0 to TR7 are indicated.

2.) reduces SIN and the low intensity 407H and 407M channels were matched using manufacturers data sheets to PMT's having the lowest dark counts. Earth loop noise pickup from the laser flash lamps was reduced by addition of a balanced isolation transformer to the Licel rack and photomultiplier power supplies and separation of laser ground. The polychromator is magnetically shielded and housed in an optically sealed enclosure. For timing a Stanford Research Systems DG535 provides the delay relative to the master trigger that is used to synchronize the Raman lidar's Nd:YAG laser with those of coexisting NDACC lidars at TMF. A further series of delays are produced via a *slaved* Quantum composer programmable timing generator to set the first range bin for all transient recorders to site altitude (2.3km) and provide the gating signal to the 355H PMT.

3.1. Correction for Geometrical Overlap

As the overlap of the 355nm beam from the Nd:YAG laser and the field of view (FOV) of the large telescope is critical for achieving maximum SNR and suppression of sky background, the 355nm laser emission is expanded by $\times 8$ via a CVI BXUV series beam expanding (BE) telescope to reduce laser divergence to 300μR. The expanded beam is then steered to optimally match the field of view of the large telescope using a micro positioning gimbal mount; the gimbal houses the beam steering mirror which also serves as a beam dump for the 532nm laser emission. The alignment system uses a modified Newport SL-A beam steering gimbal and Newfocus Pico-motors in conjunction with an 8753 controller and 8752 ethernet interface to a remote PC. The signals are monitored using a proprietary Labview alignment graphical user interface (GUI) program. The GUI allows any combination of the eight channels to be aligned automatically with dwell time (integration), number of bins summed and align altitude being configurable.

4. DISCUSSION: CALIBRATION USING SONDES

A six month climatology from April to September 2005 is shown in Figure 4 with lidar profiles integrated over a two hour period. The datasets were selected based on the closest mean times in order to reduce spatial variability between water vapor column measured by sonde and lidar. While systematic differences with radiosonde profiles are known to increase with altitude (as temperature decreases) the error between sonde and lidar profiles appears to be within the 1σ error limits of the lidar signals, indicating that the error contribution due to temperature effects on the radiosonde are within the 5% limits reported previously. With the exception of the dataset from 09/07/05 which differs significantly in the difference between the mean sonde and lidar profile times (54 mins) the plots are in excellent agreement. From the 55 datasets collected over the six month period the working maxumum altitude was between 8.5km and 18km (in July). The limits of operation of the Vaisala RS92-K radiosonde from measured temperature climatology over the same period is shown in Figure 5. An analysis of errors between sonde and lidar is shown in Figure 6. The variation between sonde and lidar profiles for the

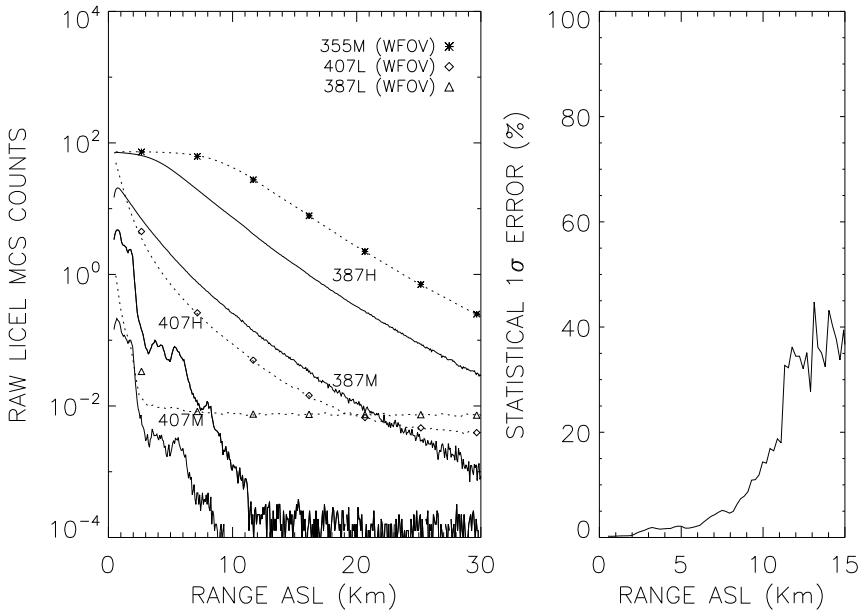

Figure 3. Raw signals from large 0.92m telescope (NFOV) and small 7.5cm telescopes (WFOV) shown dotted (left) with 1σ error shown (right) for water vapor (407nm) high range raman channel (NFOV) for this dataset only.

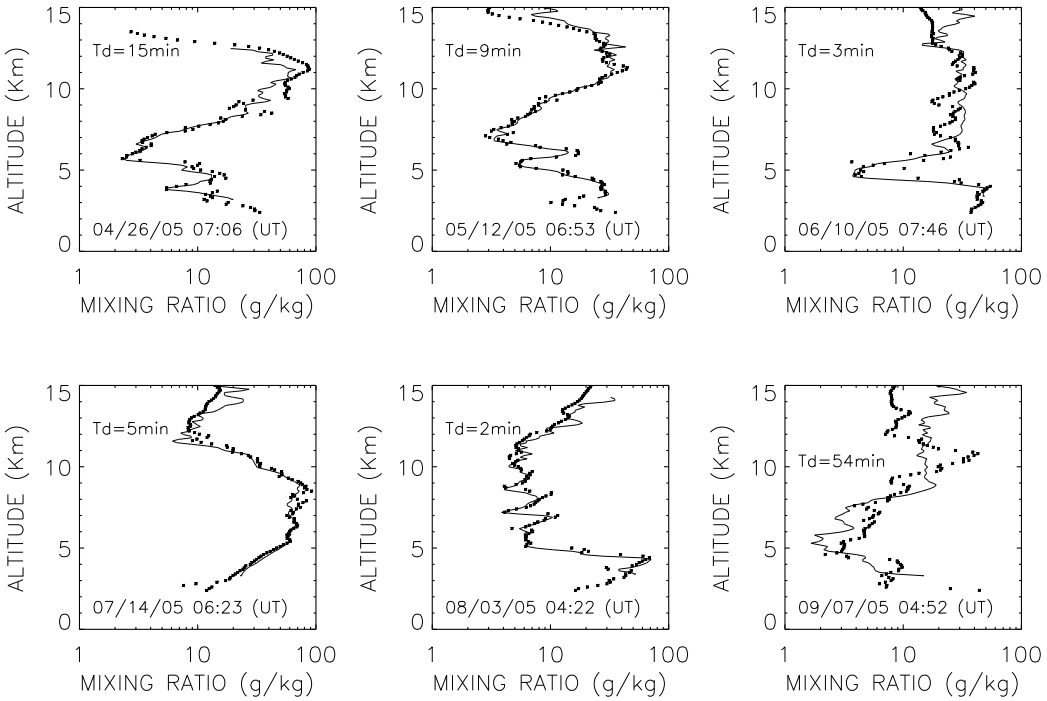

Figure 4. Climatology over six months from TMF lidar and Vaisala RS92-K radiosonde datasets.

two case studies on 07/14/05 and 04/12/05 indicates 1σ errors where the photon counting measurement error

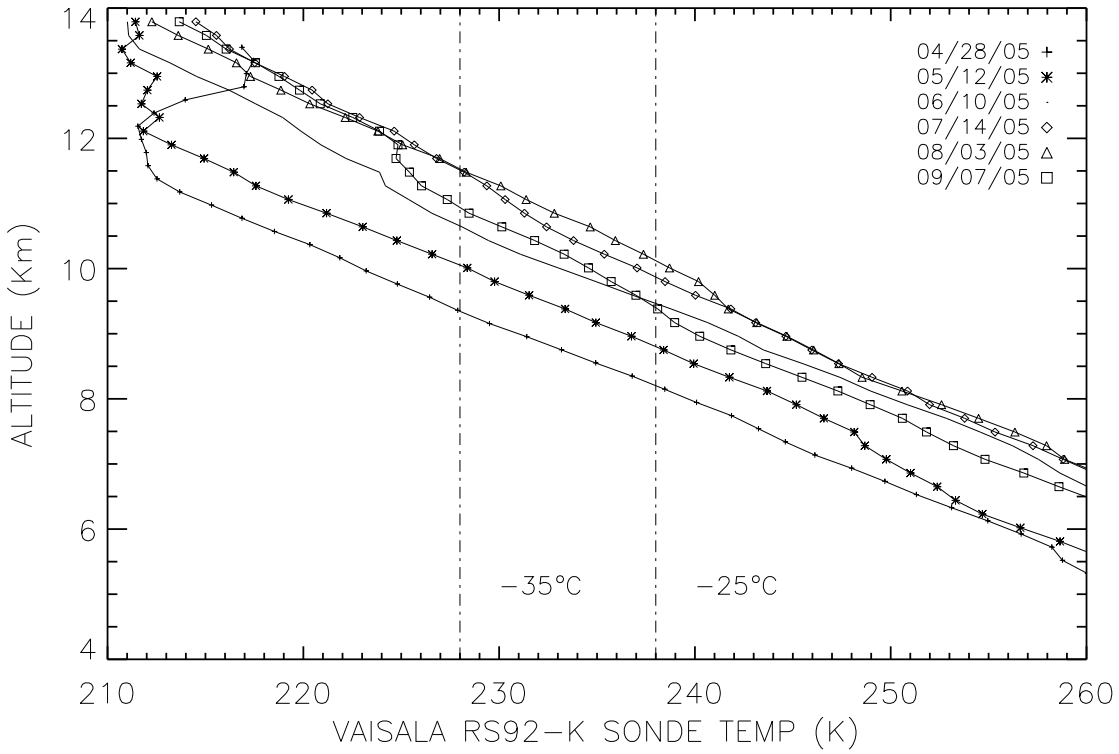

Figure 5. Temperature profiles of Vaisala RS92-K radiosondes over six month period of climatology showing altitudes corresponding to limits of accuracy of radiosonde measurements at $-35°$. Note the variation of the tropopause height with a minimum altitude at 11.5km.

follows Poisson statistics with an uncertainty given by $\Delta N = \sqrt{N}$ and where the error $E \propto 1/\sqrt{N}$.[8,23] It is seen that statistical signal error is 5% below 8km for the measurement 04/12/05 while the measurement on 07/14/05 shows significant variations below 10km possibly due to the presence of aerosol layers. As the usefulness of radiosondes for validation of lidar data is limited to temperatures above -35°C (238K) and thus altitudes below 10km, and profiles without aerosol further validations are scheduled using the GSFC AT/STROZ mobile lidars, although preliminary datasets from a previous inter comparison with the GSFC lidars are available but have not at this time been fully processed. Additional considerations are the small field of view of the lidar which makes spatial variability of measurements more likely due to variability of the water column measured as the sonde is horizontally advected and the exponential response times of sondes at altitude.

5. CONCLUDING REMARKS

The TMF Raman water vapor lidar and Vaisala RS92-K sonde profiles have been compared to produce six month water vapor and temperature climatologies for analysis purposes. While these preliminary results show overall agreement differences are evident above 10km which require further validations not possible using standard radiosondes. Differences between individual profiles from the climatology below 10km may be accounted for by the presence of aerosol layers and sonde advection. For the lowest parts of the lidar profiles it is seen that the profiles are in excellent agreement with errors typically less than 5%. Future intercomparisons planned with the mobile GSFC lidar will be used to validate the TMF lidar profiles higher up. Contrasting with the stratosphere where mixing is limited, variation of tropospheric water vapor is seen to be highly variable for the six month climatology with Summer months providing profiles to a higher altitude due to increased solar radiation causing increased water vapor column and convective forcing. This is reflected by the maximum measurement altitude for water vapor profile retrieval being 18km in July. In the mid-term the addition of the new Raman lidar to the

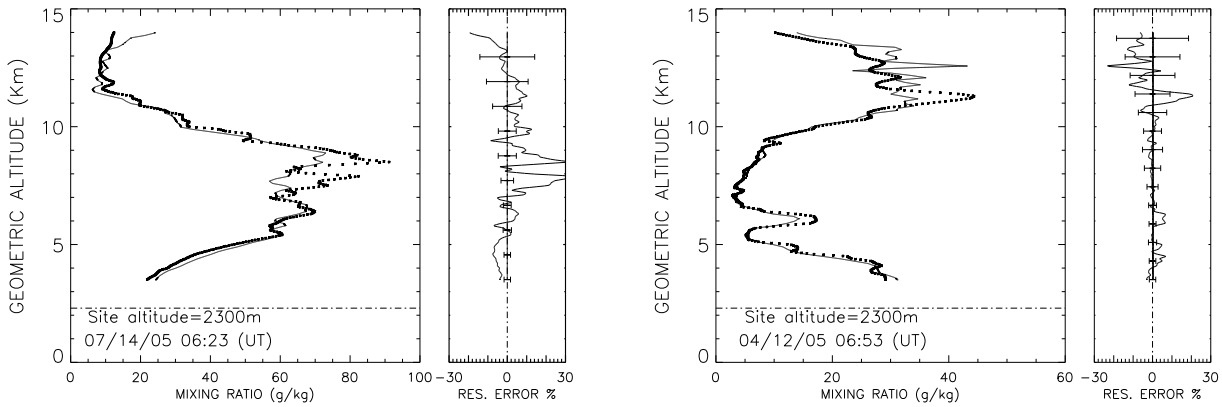

Figure 6. Error analysis for lidar and Vaisala RS92-K radiosondes showing lidar Poisson 1σ statisitical errors (bars) and relative errors between radiosonde and lidar profiles due to radiosonde inaccuracies at low temperatures and variation of radiosonde position due to advection.

exisiting co-located lidars at TMF will provide long term data for EOS-Aura satellite correlative measurements and long term reference water vapor and temperature climatology data for the NDACC archives.

6. ACKNOWLEDGMENTS

The work in this paper was carried out at Jet Propulsion Laboratory, California Institute of Technology under an agreement with the National Aeronautics and Space Administration.

REFERENCES

1. *SPARC Assessment of Upper Tropospheric and Stratospheric Water Vapor.* Report No.2, Dec. 2000. Ed. D.Kley, J.M.Russell & C.Phillips. Dec
2. A.Sinha & J.E.Harries. *Water vapor and greenhouse trapping: the role of far infrared absorption.* Geophys. Res. Lett. **22**, 2147-2150, 1995.
3. S.A.Clough, M.J.Iacono & J.L.Moncet. *Line-by-line calculation of atmospheric fluxes and cooling rates: application to water vapor.* J.Geophys. Res. **97**, 15, 761-785, 1992.
4. V.Sherlock, A.Garnier, A.Hauchecorne & P.Keckhut. *Implementation and validation of a Raman lidar measurement of middle and upper tropospheric water vapor.* Applied Optics, Vol. **38**, No. 27, Sept 1999.
5. D.Gerber, I.Balin, D.G.Feist, N.Kampfer, V.Simeonov, B.Calpini & H.van den Bergh. *Ground based water vapor soundings by microwave radiometry and Raman lidar on Jungfraujoch (Swiss Alps).* Atmos. Chem. Phys., **4**, 2171-2179, 2004
6. W.B.Grant. *Differential absorption and Raman lidar for water vapor profile measurements: a review.* Optical Engineering, Vol. **31**, No. 1, Jan 1991.
7. D.N.Whiteman. *Examination of the traditional Raman lidar technique II. Evaluating the ratios for water vapor and aerosols.* Applied Optics, Vol. **42**, No. 15, May 2003.
8. A.Behrendt. *Combined Raman Lidar for the measurement of atmospheric temperature, water vapor, particle extinction coefficient and particle backscatter coefficient.* Applied Optics, Vol. **41**, No. 36, Dec 2002.
9. D.N.Whiteman. *Examination of the traditional Raman lidar technique I. Evaluation of the temperature dependent lidar equations.* Applied Optics, Vol. **42**, No. 15, May 2003.
10. G.Vaughan, D.P.Wareing, L.Thomas & V.Mitev. *Humidity measurements in the free Troposphere using Raman backscatter.* Q.J.R.Meteorol. Soc. **114**, 1471-1484 (1988).
11. S.H.Melfi. *Remote Measurements of the Atmosphere using Raman Scattering.* Applied Optics, Vol. **11**, No. 7, July 1972.

12. J.A.Cooney. *Remote measurements of atmospheric water vapor profiles using Raman component of laser backscatter.* J.Appl. Meteorol. **9**,182-184 (1970).
13. S.H.Melfi, J.D.Lawrence & M.P.McCormick. *Observation of Raman Scattering by water vapor in the atmosphere.* Appl. Phys. Lett. **15**, 295-297 (1969).
14. V.Sherlock, A.Hauchecorne & J.Lenoble. *Methodology for the independent calibration of Raman backscatter water-vapor lidar systems.* Applied Optics, Vol. **38**, No. 27, Sept 1999.
15. D.D.Turner & J.E.M.Goldsmith. *Twenty-four-hour Raman lidar water vapor measurements during the Atmospheric Radiation Measurement program's 1996 and 1997 water vapor intensive observation periods.* J.Atmos. Ocean. Tech. **16**, 1062-1076 (1999).
16. R.A.Ferrare, S.H.Melfi, D.N.Whiteman, K.D.Evans, F.J.Schmidlin & D.Star. *A comparison of water vapor measurements made by Raman lidar and radiosondes.* J.Atmos. Ocean Tech. **12**, 1177-1195 (1995).
17. C.K.Williamson & R.J.DeYoung. *Method for the reduction of signal-induced noise in photomultiplier tubes.* Applied Optics, Vol. 39, No. 12, April 2000.
18. S.E.Bisson, J.E.M.Goldsmith & M.G.Mitchell. *Narrow-band, narrow-field-of-view Raman lidar with combined day and night capability for tropospheric water-vapor profile measurements.* Applied Optic, Vol. 38, No. 9, March 1999.
19. D.P.Donovan, J.A.Whiteway & A.Carswell. *Correction for non-linear photon-counting effects in lidar systems.* Appl. Opt. **32**, 6742-6753 (1993).
20. D.N.Whiteman, S.H.Melfi & R.A.Ferrare. *Raman lidar system for the measurement of water vapor and aerosols in the Earth's atmosphere.* Applied Optics, Vol. **31**, No. 16, June 1992.
21. F.Immler, D.Engelbart & O'Schrems. *Fluoresence from atmospheric aerosol detected by a lidar indicates biogenic particles in the lowermost stratosphere.* Atmos. Chem. Phys., **5**, 345-355, 2005.
22. A.Ansmann, M.Riebesell & C.Weitkamp. *Measurement of atmospheric aerosol extinction profiles with a Raman lidar.* Optics Letters, Vol. **15**, Bo. 13, July 1990.
23. A.Behrendt, T.Nakamura & T.Tsuda. *Combined temperature lidar for measurements in the troposphere, stratosphere and mesosphere* Applied Optics, Vol. **43**, No. 14, May 2004.